Vegetation structure and soil organic carbon storage across northern forest-tundra ecotones in continuous permafrost

H. Travers-Smith, N.C. Coops, Trevor C. Lantz, M. Hamp, D. Ignace, M.A. Wulder, & J. van der Sluijs

2025

Original citation:

Travers-Smith, H. Z., Coops, N. C., Lantz, T. C., Hamp, M., Ignace, D., Wulder, M. A., & Van Der Sluijs, J. (2025). Vegetation structure and soil organic carbon storage across northern forest-tundra ecotones in continuous permafrost. *Arctic Science*. https://doi.org/10.1139/as-2024-0048

Arctic Science

OPEN ACCESS | Research Article

Vegetation structure and soil organic carbon storage across northern forest-tundra ecotones in continuous permafrost

H. Travers-Smith[a], **N.C. Coops**[a], **T.C. Lantz**[b], **M. Hamp**[b], **D. Ignace**[c], **M.A. Wulder**[d], and **J. van der Sluijs**[e]

[a]Department of Forest Resource Management, University of British Columbia, Vancouver, BC V6T 1Z4, Canada; [b]School of Environmental Studies, University of Victoria, Victoria, BC V8W 2Y2, Canada; [c]Department of Forest Resources, University of Minnesota, St. Paul, MN 55108, USA; [d]Canadian Forest Service, (Pacific Forestry Centre), Natural Resources Canada, Victoria, BC V8Z 1M5, Canada; [e]Northwest Territories Centre for Geomatics, Yellowknife, NT, Canada

Corresponding author: **H. Travers-Smith** (email: hanats@student.ubc.ca)

Abstract

Climate change is altering northern vegetation structure and below-ground carbon storage. Expanding forest and shrub cover has decreased soil organic carbon (SOC) storage in some parts of the forest-tundra ecotone. In this study, we linked measurements of SOC with terrain and vegetation structure derived from drone imagery across treelines underlain by continuous permafrost in the Northwest Territories, Canada. We classified sites into three treeline types representing differences in vegetation productivity and topography. Between treeline types, we observed differences in C:N ratios and organic matter depth related to the rate of soil carbon turnover and SOC storage. Overall, SOC showed small positive relationships with tree stem density and average canopy height. We did not find evidence that expanding tree- and shrublines would result in losses of SOC storage in our study area. Instead, topography and landscape drainage patterns, rather than vegetation structure may be more important predictors of SOC storage. We used medium resolution satellite data to extend predictions of treeline type across our study area. The majority of predicted treelines (82%) showed positive relationships between vegetation height and SOC storage. Our findings highlight the value of integrating vegetation structure and landscape features in understanding carbon dynamics in the forest-tundra ecotone.

Key words: soil carbon, treeline, vegetation structure, drone, Remotely Piloted Aircraft System, Landsat

Introduction

Approximately half of the world's soil organic carbon (SOC) is stored at high latitudes (Tarnocai et al. 2009) and is vulnerable to release due to climate warming, permafrost thaw, and microbial decomposition (Rodionov et al. 2007; Miner et al. 2022). However, climate warming can also change litter inputs and increase vegetation productivity, which may offset carbon losses from the soil (Cornelissen et al. 2007; Sistla et al. 2013). Earth system models of carbon dioxide fluxes suggest that high latitude ecosystems are currently carbon sinks, with more carbon sequestration observed in the boreal biome compared to the tundra (McGuire et al. 2012; Virkkala et al. 2021). These models, however, show a high level of uncertainty in predicting future changes due to our limited understanding of the distribution of soil carbon pools in boreal and tundra ecosystems and the drivers of primary productivity and ecosystem respiration (Virkkala et al. 2021). In particular, field studies suggest that the current models of soil carbon storage may not adequately account for carbon release following northward (latitudinal) and upward (elevational) shifts in treelines and shrublines (Wilmking et al. 2006; Street et al. 2020; Clemmensen et al. 2021).

At high latitudes, the majority of ecosystem carbon is stored in soils and permafrost rather than above-ground biomass (Wilmking et al. 2006; Siewert et al. 2015). Previous work across European alpine treelines show that tundra heath can store up to two times more carbon than adjacent birch forests due to large soil carbon pools (Hartley et al. 2012; Parker et al. 2015, 2021; Clemmensen et al. 2021; Kemppinen et al. 2021). Similarly, in the Alaskan forest-tundra ecotone, Wilmking et al. (2006) reported larger ecosystem carbon pools in tussock tundra sites compared to nearby forested woodlands. These observations have been attributed to limited drainage and organic matter accumulation in tundra soils (Wilmking et al. 2006), as well as variation in plant communities and associated mycorrhizal fungi (Clemmensen et al. 2021). In some cases, the expansion of trees and deciduous shrubs into the tundra have been shown to accelerate soil carbon turnover and respiration rates due to rhizome priming effects (Clemmensen et al. 2015; Parker et al. 2015; Street et al. 2020). In contrast, sedge and evergreen shrubs characteristic of tundra heath ecosystems can increase soil carbon storage by creating stable pools of below-ground necromass (Clemmensen et al. 2021). Parker et al. (2021) have suggested that soil carbon losses following treeline and shrubline advance could be an order of magnitude greater than gains in carbon storage from increasing plant productivity and above-ground biomass.

However, some studies assessing the impact of climate warming on above and below-ground carbon storage along latitudinal treelines and within continuous permafrost have found no significant changes in soil carbon pools, despite increases in litterfall (Ziegler et al. 2017), above-ground biomass, and shrub density (Sistla et al. 2013). Devos et al. (2022) assessed differences in carbon storage between forest and tundra soils across a 500 km latitudinal transect in Norway and found that forested soils had slightly higher mean SOC storage compared to tundra soils, albeit with substantial variation between site types. These findings suggest that factors other than vegetation composition such as microtopography (Zona et al. 2011; Pichler et al. 2022), landform type (Wojcik et al. 2019), or permafrost stability (Robinson and Moore 2000; Siewert et al. 2015) may drive fine-scale variation in SOC storage across latitudinal treelines.

To date, many studies comparing ecosystem carbon pools in forests and tundra sites have been conducted in alpine regions without permafrost (Hartley et al. 2012; Clemmensen et al. 2015, 2021; Parker et al. 2015, 2021; Sørensen et al. 2018), or in discontinuous and sporadic permafrost (Wilmking et al. 2006; Ziegler et al. 2017; Devos et al. 2022). The relative lack of treeline studies conducted in continuous permafrost limits our ability to predict the consequences of widespread vegetation changes on soil carbon storage across the circumpolar region (see Rodionov et al. 2007; Sistla et al. 2013; Siewert et al. 2015; Wojcik et al. 2019). Given widespread changes in vegetation structure in forest-tundra ecotone (Myers-Smith and Hik 2018; Hansson et al. 2021), there is a need for improved monitoring of changes in both above and below-ground carbon storage and the ability to characterize soil carbon dynamics using vegetation composition and structure.

Integrating field-based methods with remote sensing can improve our understanding of the composition and structure of high-latitude vegetation (Castilla et al. 2022; van der Sluijs et al. 2023*a*) as well as topographic controls on soil carbon storage (Kokelj et al. 2007; Thomas et al. 2023). Drones can be used to generate three-dimensional models of terrain and vegetation structure at high spatial resolution (Fraser et al. 2016). In addition, imagery from drones can be used to scale between field measurements and medium spatial resolution (10–100 m) satellite data (Orndahl et al. 2022), which provide global coverage and can be used to detect long-term landscape changes (Fraser et al. 2017; Castilla et al. 2022). Several recent studies have used spectral greenness indices such as the Normalized Difference Vegetation Index, Enhanced Vegetation Index (EVI) (Berner and Goetz 2021), or global models of tree cover including the Landsat and MODIS Vegetation Continuous Fields datasets to assess changes in forest cover and structure at the treeline (Montesano et al. 2020). However, more work is needed to understand how variation in spectral indices from optical satellite platforms correspond with fine-scale vegetation structure and cover across regional tree- and shrublines (Loranty et al. 2018; Walker et al. 2021; van der Sluijs et al. 2023*a*).

In this analysis, we assessed relationships between SOC storage, microtopography, and vegetation structure across differing treeline types underlain by continuous permafrost in northwestern Canada. Widespread shrub expansion has been documented throughout this region (Lantz et al. 2010; Fraser et al. 2014*a*; Moffat et al. 2016). While the northern position of the treeline has remained stable over time (Timoney and Mamet 2020), stand density has increased at sites below the treeline (Lantz et al. 2019; Travers-Smith and Lantz 2020). Thus, our study area is representative of changes in tree density and shrub growth occurring within the forest-tundra ecotone. We collected drone surveys, vegetation, and soil data across 11 transects representing the transition from open spruce woodlands to shrub and tussock tundra. These transects were grouped into three treeline types representing differences in drainage characteristics and overall site productivity. At each transect, we collected samples of the organic soil horizon ($n = 155$) and plot-scale vegetation surveys ($n = 55$). High-resolution drone surveys of each transect were used to map vegetation height and microtopography, which were spatially associated with the plot-level vegetation and soil data. We used these data to test the hypothesis that increasing vegetation height and forest density is correlated with decreasing SOC storage within and across treeline types. Finally, we used Landsat imagery and topographic data to predict the frequency of the three treeline types across unsampled treelines in our study area.

Methods

Study area

Our study area is in the western Canadian Arctic within the Caribou Hills Ecoregion of the Northwest Territories (Fig. 1; Ecosystem Classification Group 2012). This area is located in the Inuvialuit Settlement Region and is between the nearby communities of Inuvik and Tuktoyaktuk. The Caribou Hills Ecoregion is underlain by continuous permafrost and is a transitional area between the High Subarctic ecozone in the south and the Low Arctic in the north (Ecosystem Classification Group 2012). This region is lake-rich and is characterized by rolling morainal deposits consisting of till and associated gravel and sand deposited by glacier ice (Rampton 1988). Vegetation across the ecoregion consists of open white spruce woodlands and low-shrub tundra that gradually transitions to tussock-sedge and dwarf-shrub tundra in the Low Arctic (Ecosystem Classification Group 2012). The dominant tree species at our sites was white spruce (*Picea glauca* (Moench) Voss). Upright shrub species included willow (*Salix* ssp. L.), birch (*Betula glandulosa* Michaux), and green alder (*Alnus viridis* ssp. *fructicosa* (Ruprecht) Nyman). The most common understory herbs and dwarf shrubs were bog bilberry (*Vaccinium uliginosum* L.), kinnikinnick (*Arctostaphylos alpina* ssp.

Fig. 1. Map of the study area in northwestern Canada. Transects were established along the Inuvik–Tuktoyaktuk highway (left). At each transect (n = 11) we acquired soil samples (n = 15) and concurrent drone imagery at 1 cm spatial resolution (right). The image to the right shows the location of soil samples at the transect marked with an arrow. The inset map (top-left) shows the study area in relation to the tree limit and forest-tundra ecotone mapped by Timoney et al. (1992).

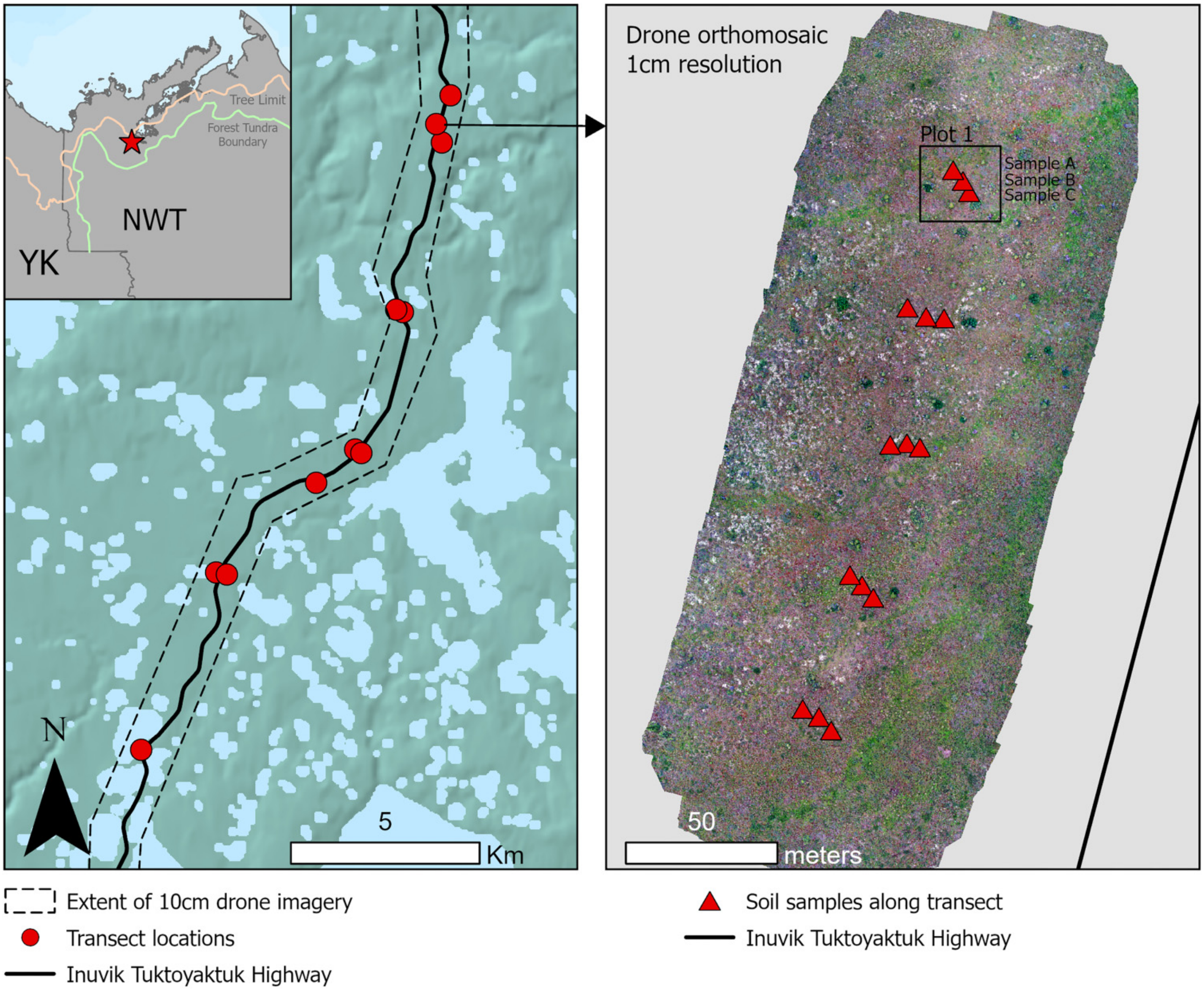

rubra (Rehder & Wilson) Hultén), and crowberry (*Empetrum nigrum* L.).

Field sampling was conducted at undisturbed treeline sites adjacent to the Inuvik–Tuktoyaktuk Highway (ITH), north of Inuvik. All field sites lie between the southern boundary of the forest-tundra and northernmost tree limit (Fig. 1; Timoney et al. 1992). Sites were selected to represent "local" treelines using high-resolution satellite imagery showing small spruce woodlands. Average annual air temperature recorded at Inuvik between 1970 and 2016 was −8.6 °C (ECCC 2024). Using measurements recorded in Inuvik and Aklavik, between 1926 and 2016, annual and summer air temperatures have warmed by 3.5 and 1.9 °C, respectively (Lantz et al. 2019). In addition to climatic changes, the construction (2014–2017) and ongoing use of the all-season gravel highway may also impact the surrounding tundra environment by driving earlier snowmelt (Hammar et al. 2023) and increasing soil nutrient availability and moisture (Gill et al. 2014).

Overall workflow

This section provides an overview of the workflow used in this research and additional detail is provided in the sections that follow (Fig. 2). Data collection was divided into three parts, representing nested spatial scales of analysis, (1) fine-scale soil and vegetation sampling within 11 treeline sites, (2) intermediate scale drone imagery (1 cm spatial resolution) of each treeline site, and (3) landscape scale spectral and topographic indices from Landsat imagery (30 m) and a second drone acquisition of the entire ITH. After data collection, we grouped the treeline sites (n = 11) into three site types Moist Tundra (MT), Mesic Woodland (MW), and Submesic Woodland (SW) using clusters in Landsat spectral indices and topographic variation within each site. Plot level cover of vegetation functional groups (n = 55) was used to evaluate ecological differences among the treeline types.

The second part of data analysis combined the plot level soil data with the high spatial resolution drone imagery to

Fig. 2. Flow chart of the primary steps in the data analysis and associated outputs. As noted in the key, the color and shading of the boxes indicate which data source and scale was used to derive each output.

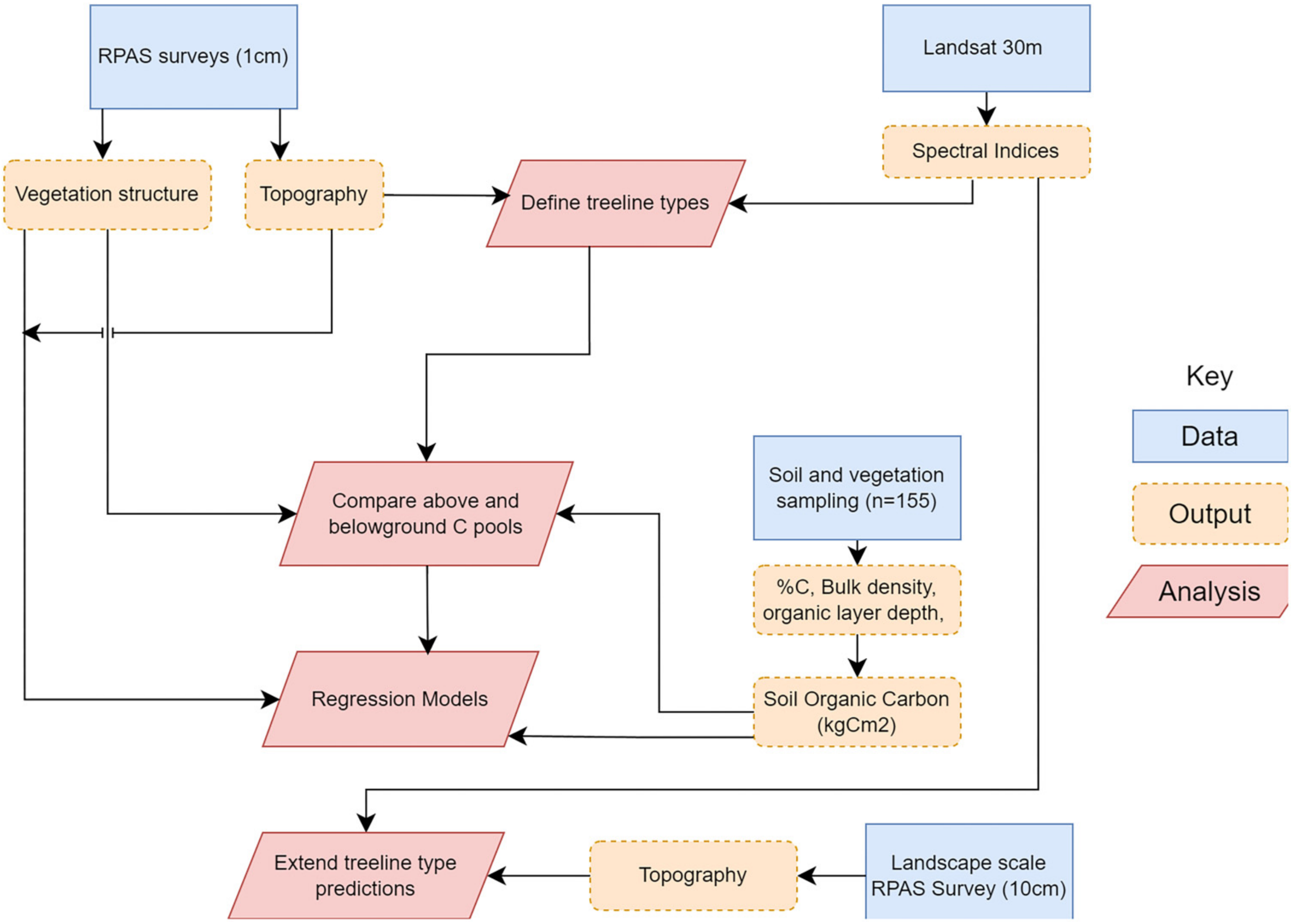

compare variation in above and below-ground carbon storage among treeline types and model soil carbon storage as a function of microtopography and vegetation structure. At each site, we collected 15 soil samples (three per plot) along 200 m transects that extended across the treeline. For each soil sample, we measured carbon content (%), soil bulk density (kg m^{-3}) and SOC (kg C m^{-2}) and recorded the depth of the organic horizon and litter layer. From the drone imagery, we derived terrain and canopy height models (CHMs), using photogrammetry (Westoby et al. 2012; Fraser et al. 2016) which were spatially aligned with the locations of the soil samples. We then developed linear regression models to predict soil carbon content, bulk density, and organic carbon storage using the drone-derived terrain and CHM data.

After characterizing above and below-ground carbon storage across treeline types, the third component of data analysis extended predictions of treeline types to similar, but unmapped sites within our study area. To do this, we used the clustering analysis to predict the most likely site type for 21 km of additional treelines using Landsat spectral indices and topographic metrics from the landscape scale drone acquisition of the ITH.

Data description

Field data collection

At each site we delineated a 200 m transect crossing the local treeline and sampled vegetation plots at 50 m intervals along the transect (Fig. 1). At each of the five plots, a single observer recorded the percent cover of plant functional groups within nested 3 and 1 m^2 quadrats. In the 3 m^2 quadrat we estimated the percent cover of tree and upright shrubs (*Betula*, *Alnus*, *Salix*). In the 1 m^2 quadrat we estimated percent cover of dwarf shrubs (*Empetrum*, *Vaccinium*, *Arctostaphylos*) herbs, graminoids, moss, lichen, and litter.

All soil and vegetation surveys were conducted between 15 July and 26 July 2023. At each plot we collected triplicate soil samples (A, B, and C). Sample B was always placed in the center of the 1 m^2 vegetation plot, while samples A and C were randomly spaced 2–3 m apart on either side of each vegetation plot (Fig. 1). Soil carbon was quantified by extracting a monolith of the unfrozen organic horizon to the depth of the mineral horizon or to permafrost using a small shovel and knife. From the extracted material we cut a vertical profile to represent a composite of organic material in the active layer. The pit dug to extract the monolith was then used to measure the thickness of the organic layer (m) either to the mineral layer or to permafrost. Samples of the organic horizon were subsequently frozen and shipped to the Stable Isotope Facility at the University of British Columbia for analysis. At the location of each soil sample, we also recorded active layer depth, litter layer depth, and the depth of the organic horizon, measured from the top of the soil horizon to mineral soil or to permafrost to the nearest cm. In cases where mineral soil was mixed into the surface organic horizon, we estimated the ratio of mineral to organic soil using color and texture. To locate soil samples within the drone imagery, soil pits were filled and covered by brightly colored discs that were easily discernable in the imagery.

Laboratory analysis of soil C and N content

After collection in the field, soil samples were kept frozen until analysis for carbon and nitrogen content. Samples were completely dried in an oven at 60 °C for 3 days. After drying, large twigs and roots were removed and discarded. The soils were sieved to <2 mm and homogenized using a mortar and pestle. The bulk density was calculated as the weight of the dry soil divided by the volume of the sample. A small amount of soil (5 mg) was then sampled and sent to the Stable Isotope Facility for analysis. Samples were measured in an elemental analyzer (Elementar Vario EL Cube; in C, N mode, Hanau, Germany) for carbon and nitrogen content (C% and N%).

SOC stocks were calculated using laboratory and field measurements in the following equation (Parker et al. 2021; Devos et al. 2022):

SOC ($\mathrm{kg\ C\ m^{-2}}$) = C content (%) × Bulk density ($\mathrm{kg\ m^{-3}}$) × Depth of organic horizon (m).

The final SOC measurement is an estimate of the amount of carbon stored in the unfrozen organic horizon at the time of sampling, per unit area. SOC stocks may be underestimated for samples where we were not able reach the mineral horizon due to permafrost ($n = 36$).

Drone surveys and photogrammetry

We used WorldView-2 imagery from the satellite base maps in ArcGIS Pro to identify treelines accessible from the highway. Treeline transitions were defined as sites containing tree stems visible in WorldView-2 imagery transitioning to adjacent areas with none or only a few tree stems visible. We restricted sampling to undisturbed sites north of the 1:1 forest-tundra boundary defined by Timoney et al. (1992) and did not sample areas where the trees were obviously limited by water features or steep topography. Sites were selected to represent a range of topographic and environmental conditions and were placed at least 200 m apart from each other.

For each transect, aerial images used to model canopy height were captured using the DJI Mavic 2 Pro flown at 40 m altitude, producing a pixel resolution of 1 cm. Surveys were centered on the treeline transects and were approximately 250 m in length and 100 m in width (Fig. 1). The Mavic 2 Pro is equipped with an RGB camera flying in a grid pattern. The camera was triggered at equal distance intervals with front and side overlap of 80% and 70%, respectively (Fraser et al. 2017). We used Agisoft Metashape Professional (v.1.8.3) to generate dense point clouds in each area surveyed. Images were aligned using a key point limit of 40 000 and a tie point limit of 4000 and were optimized using adaptive camera model fitting (Fraser et al. 2016). In the image alignment step, processing with “High” accuracy produced unrealistic curvature at the edges of the survey, thus we used the “Low” accuracy alignment, which resulted in fewer tie-points but removed “doming” effects in the Digital Terrain Model (DTM). Point clouds were generated using “High” accuracy and processed further in R Statistical Software (v.4.4.1; R Core Team 2022) using the lidR package (Roussel et al. 2020). The full pointclouds had an approximate point density of 2200–2700 points per m^2. As no ground control points were used to improve the absolute georeferencing of the data, the expected horizontal offset of the point clouds was 5–10 m based on comparison of the orthomosaics with georeferenced basemaps. As this positional error is less than or similar to registration accuracy of Landsat (one half pixel; <15 m), it is not expected that the spectral comparison and scaling used in this work was impacted (Storey et al. 2014; Fraser et al. 2017).

We used the cloth simulation function in the lidR package to classify points into ground and canopy classes using a class threshold of 0.25 m, the default cloth resolution and a cloth rigidness parameter of three (more rigid). A Digital Elevation Model (DEM) was generated at 1 m resolution by interpolating the ground classified points, which had an approximate density of 55–60 points/m^2. From the DEM, we used the raster package in R (Hijmans 2022) to calculate slope, roughness, and Topographic Position Index (TPI) at 1 m resolution to represent site microtopography. Points classified as vegetation canopy were normalized to the DEM and rasterized CHMs were generated at 10 cm resolution using the maximum height of the normalized point cloud within each pixel. We provide validation data for canopy height using drone-derived CHMs within our study area in the Supplementary Material. From the CHM, the locate_trees function in the lidR package was used to identify local height maxima and map individual tree stems in each survey. The function was parameterized using the local maximum filter with a minimum height of 2.5 m and a window size of 2 m. Tree stem density was calculated as the number of stems >2.5 m divided by the drone survey area. This threshold was selected to conservatively estimate the number of mature white spruce stems that would contribute most to total above-ground biomass. Smaller seedlings would be included in our estimates of tall shrub and understory biomass.

Landscape scale data

We used annual Landsat Best Available Pixel (BAP) composites to calculate a suite of spectral indices at 30 m spatial resolution. BAP composites are cloud and gap-free mosaics of surface reflectance generated at an annual time-step using data from Landsat-5, 7, and 8 (Hermosilla et al. 2015). Composites

Table 1. Landsat and topographic variables used to define treeline types within a k-means clustering algorithm.

Variable name	Site scale aggregation
Tasseled Cap Wetness	Mean of 30 m pixels
Tasseled Cap Greenness	Mean of 30 m pixels
Tasseled Cap Brightness	Mean of 30 m pixels
Enhanced Vegetation Index	Mean of 30 m pixels
Slope mean	Mean of slope in 30 m pixels
DTM range	Range in elevation in 30 m pixels
DTM standard deviation	Standard deviation of elevation in 30 m pixels

Note: Variables at 30 m resolution were aggregated to the transect scale representing an area approximately 250 × 100 m (~27 pixels).

are created from multiple images acquired over a single growing season, and pixel scoring functions are used to select the best pixel based on sensor, acquisition day, distance to clouds, cloud shadow, and atmospheric opacity (White et al. 2014). For the 10-year period between 2012 and 2022, we calculated the median annual Tasseled Cap Greenness (TCG), Tasseled Cap Wetness (TCW), Tasseled Cap Brightness (TCB), and the EVI. Spectral indices were calculated using the equations in Hermosilla et al. (2022). TCW was originally defined to correspond to soil moisture in areas occupied by bare soil (Kauth and Thomas 1976), whereas in sparsely forested areas higher TCW can reflect the presence of coniferous trees (Fraser et al. 2014*b*).

To extend predictions of treeline type over the entire study area, we used data from a drone acquisition along the ITH collected at 10 cm spatial resolution (van der Sluijs et al. 2023*b*). Data consisted of point clouds previously processed with photogrammetry and validated against ground and remotely sensed terrain and vegetation height information (van der Sluijs et al. 2024). From these point clouds, we classified ground and canopy points using the lidR package using the same cloth simulation function described previously. The class threshold and cloth resolution were set to 1 m and cloth rigidness set to 3. From the ground points, a 1 m DEM as well as slope and TPI was generated over the entire highway corridor.

Data analysis

Defining treeline types

To compare the relationships between vegetation structure and carbon storage in different site types, we grouped the 11 treeline transects into 3 treeline classes representing differences in vegetation productivity, soil and canopy moisture, and topography. Clustering was performed using a k-nearest neighbor algorithm across four Landsat indices (EVI, TCG, TCB, TCW) as well as variation in topography across each transect (Table 1). Transect-scale topography was estimated by aggregating the 1 m topographic metrics derived from the drone surveys to 30 m resolution using the mean value within each pixel, and calculating site scale variation in elevation and slope. Clustering was performed in R using the cluster package (Maechler et al. 2022), and all data were standardized before analysis. To visualize the cluster centroids, we used a principal component analysis to reduce the input variables to two dimensions and calculated the variance explained by each dimension using the factoextra package (Kassambara and Mundt 2020; Supplementary Material).

Assessing drivers of soil carbon storage using drone data

We assessed differences in above-ground biomass, SOC storage, C:N ratio, active layer depth, litter layer depth, organic layer depth, and bulk density among the three treeline site types using one-way ANOVA and Tukey test for pairwise comparisons. Comparisons were performed using soil samples with less than 30% mineral fraction ($n = 140$), as samples with high mineral content came from cryoturbated areas with frost boils and did not represent the organic horizon (Kokelj et al. 2007). To evaluate changes in SOC across treeline transects, we used maps of tree stems (>2.5 m) to determine stem density within circular 30 m plots of each soil sample. Soil samples were ordered and binned according to variation in tree stem density. In some cases, the one-way ANOVA indicated a statistically significant ($p < 0.05$) difference in mean values, but the Tukey pairwise comparisons did not. We first report p values for the one-way ANOVA and then include mean values for each site type with the associated p values for specific pairwise comparisons.

We used Ordinary Least Squares regression to compare fine-scale vegetation and topographic drivers of soil carbon content (%), soil bulk density (kg m^{-3}), and SOC storage (kg C m^{-2}) within treeline types. Histograms of each input variable were examined prior to modeling, and variables exhibiting right-skewed distributions were log-transformed to approximate a normal distribution. Input variables included vegetation structure and microtopography derived from photogrammetry and field-measurements of litter layer depth. The vegetation structure metrics used in this analysis were generated by creating a 3 m circular buffer around soil sample locations and calculating the mean, maximum, and standard deviation in canopy height within the buffer. Topographic metrics, including slope, aspect, TPI, and roughness were derived from the 1 m DTM and were extracted from the pixel intersecting with the location of the soil sample. Stepwise variable selection was used to minimize the Akaike Information Criterion (AIC) and fit parsimonious models for each response variable. We fit a global model as well as models within each treeline type. We used the statistical significance of model coefficients to assess the relative importance of vegetation structure, litter, and topographic controls on soil carbon storage.

Modelling above-ground biomass and carbon storage

We used the CHMs derived from drone to estimate above-ground biomass and below-ground carbon storage within trees and understory shrubs. To estimate tree biomass, we used a public dataset of destructively sampled trees across

Table 2. Mean above and below-ground carbon storage summarized by treeline type.

Cluster	Tree C (kg C m^{-2})	Shrub C (kg C m^{-2})	Total C (kg C m^{-2})	Active layer depth (cm)	C:N ratio	Depth of organic (cm)	Litter layer depth (cm)	C content (%)	Bulk density (kg m^{-3})	SOC kg C (m^{-2})
1 MT ($n = 46$)	0.006*	0.111	0.117	41.0	25.3*	17.6	0.6*	38.1	256.9	15.8*
2 MW ($n = 59$)	0.031*	0.091	0.122	49.2	20.3*	14.9	0.4*	36.1	306.0	16.3*
3 SW ($n = 40$)	0.043*	0.189	0.232	48.2	22.6*	13.4	0.8*	38.0	288.1	14.5*
Global ($N = 145$)	0.025*	0.108	0.133	46.3	22.5*	15.3	0.6*	37.3	285.5	15.6*

Note: Asterisks (*) indicate where there were significant ($p < 0.05$) differences between treeline types. Note that total above-ground biomass was calculated from each drone survey and averaged by treeline type ($n = 11$). SOC, soil organic carbon; MT, Moist Tundra; MW, Mesic Woodland; SW, Submesic Woodland.

Canada to model the relationship between stem height (m) and dry biomass (kg; Ung et al. 2017). From the dataset of 9000 trees, we extracted white spruce (*Picea glauca*) samples from the Northwest Territories and Yukon Territory less than 10 m tall ($n = 118$). We used the following nonlinear regression model commonly used to estimate tree biomass (Flade et al. 2020): $y = \beta x^{\alpha}$. The best-fit coefficients for the parameters β and α were found using the nls function in R. From this model, we estimated dry biomass (kg) for each tree stem in our drone surveys greater than 2.5 m in height ($n = 2343$). Carbon content was calculated as 50% of total dry biomass weight (Wilmking et al. 2006).

To estimate shrub and understory biomass we used a linear model relating canopy volume (m^3) derived from Terrestrial Laser Scanning to harvested biomass (g) from similar tundra shrub communities near Toolik Lake, Alaska (Greaves et al. 2017). To avoid counting tree biomass twice, we masked trees from the CHM using a 1.5 m circular buffer around mapped tree stems. We then converted canopy height to canopy volume by multiplying by the pixel area (25 cm^2). For each drone survey, total canopy volume was calculated as the sum of all 25 cm^2 pixels. Total biomass within each survey was calculated using the following regression equation (Greaves et al. 2017): biomass (g) $= -180 + 2485 \times$ canopy volume (m^3). Greaves et al. (2017) reported a root mean square difference of 106 g for this model. Carbon content was also assumed to be 50% of modelled biomass (Wilmking et al. 2006).

Comparing satellite vegetation indices with drone vegetation metrics

Above-ground biomass, vegetation height, and productivity may be useful explanatory variables to characterize site-level SOC storage (Clemmensen et al. 2015; Parker et al. 2015), thus the ability of medium resolution satellite imagery to extrapolate these variables is an important consideration. To evaluate the sensitivity of Landsat satellite imagery to fine-scale variation in vegetation cover and structure in the forest-tundra ecotone, we compared drone-derived metrics of productivity, tree density, and maximum stand height to spectral indices derived from Landsat imagery. The Excess Greenness (ExG) index uses the RGB channels of a standard camera and is a proxy for greenness indices derived from multispectral sensors, calculated as: 2 × Green—(Red + Blue) (Richardson et al. 2007). In northern boreal forests, it was found to be the strongest discriminator between green vegetation and background signals (Fraser et al. 2017). We calculated ExG from the drone orthomosaics and aggregated to 30 m spatial resolution using the mean value of each pixel. Stem density was calculated as the number of stems >2.5 m within each Landsat pixel, divided by pixel area (900 m^2). Maximum height was calculated by aggregating the CHM to 30 m using the maximum value within each pixel. We assessed the ability of Landsat indices (TCB, TCW, TCG, EVI) to predict the ExG index, tree stem density, and maximum canopy height from fine-scale drone imagery using Generalized Additive Models (GAMs) and extracting model r^2 and room mean square error (RMSE). GAMs were fit with a smooth term for the predictor variable using cubic regression splines and three knots (which determine the type of smoothing algorithm and the degree of smoothing).

Predicting treeline types

We mapped and classified unsampled treelines within the study area using k-means clusters to predict new treeline types (Hartigan and Wong 1979). We used the satellite imagery base maps in ArcGIS Pro to manually digitize all treelines applying the same criteria used to identify survey locations. Sample points were generated at 200 m intervals along the treelines, and at each point we generated 200 m transects running perpendicular across the treeline. Transects were buffered 50 m on either side to form rectangular sample areas of comparable size to the initial drone surveys. Due to the geometry of the treelines, some sample areas were removed if they overlapped significantly with neighbouring areas. This process retained 35 sample areas representing 70 ha for further classification. Within each sample area we extracted Landsat spectral indices as well as metrics of variation in elevation and slope (Table 2) from the landscape scale drone data at 30 m resolution. We used the k-means clustering model in the "stats" R package (R Core Team 2022) to assign treeline types to new samples using the minimum distance to cluster centroids.

Results

Characterizing treeline types

To test for site-level differences in above and below-ground carbon storage, the 11 treeline transects were clustered into ecological types based on variation in topography and Landsat spectral indices across each transect. The first two

Fig. 3. Boxplots of Landsat indices and topographic variation within three landscape clusters (Moist Tundra, Mesic Woodland, and Submesic Woodland), classified using a k-mean clustering algorithm. Note that stem density was not used to cluster treeline types but is shown to contextualize differences in treeline types. EVI, Enhanced Vegetation Index; TCG, Tasseled Cap Greenness; TCW, Tasseled Cap Wetness.

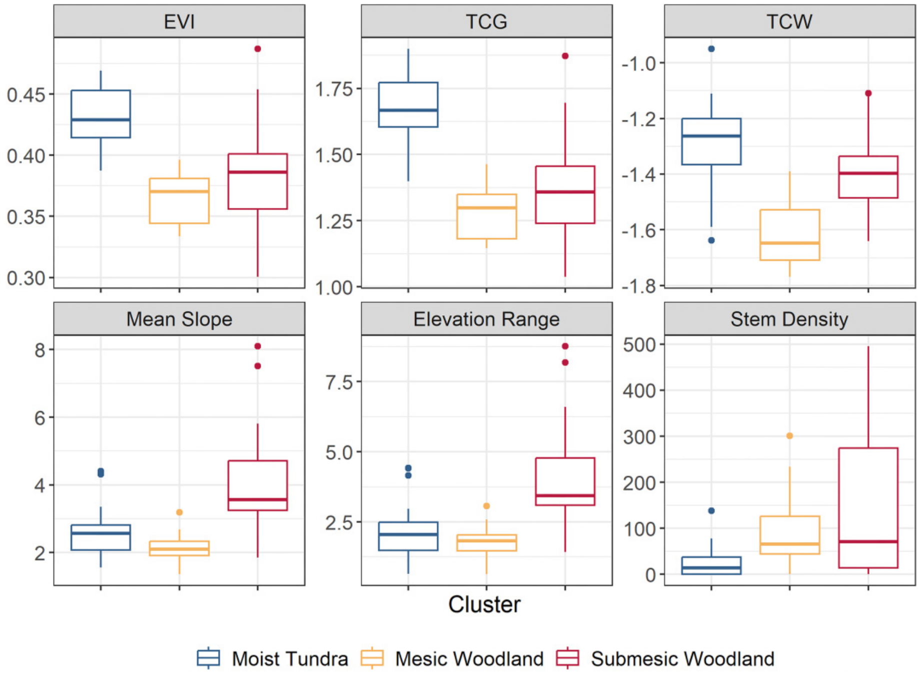

dimensions of the principal component analysis explained 89% of the variation in the input variables, with the first dimension reflecting variation in slope and elevation and the second dimension reflecting differences in TCG, TCW, and EVI. Based on these characteristics, in the following text we define treeline types as MT, MW, and SW. The first treeline type (MT) contained four transects, which were characterized by high spectral greenness and wetness and low topographic variation (Fig. 3). Vegetation communities were characterized by willow and green alder, and the median percent cover of shrubs was 29.5% (Fig. 4). Median tree cover and stem density was also low compared to other sites with 14 stems/ha. Topography was relatively uniform across this site type, with a median range of elevation of 2.04 m. The second treeline type (MW) contained four transects, which were characterized by low spectral greenness and wetness (Fig. 3). This site type was characterized by moderate tree stem density (65 stems/ha) with low median shrub cover (12.5%) and a significant moss and graminoid understory (30% and 17.5% cover, respectively; Fig. 4). Topographic relief was similar to the MT sites with 1.88 m of elevation change. The final treeline type (SW) contained three transects and was characterized by high topographic variation and slope with moderate spectral greenness and wetness (Fig. 3). The median change in elevation was 3.44 m with slopes 47% greater than the other two treeline types. Similar to the MW sites, SW sites also had high median tree stem density (71 stems/ha), but the understory was composed primarily of dwarf shrubs (53% median cover), instead of mosses and graminoids (5% and 12%, respectively; Fig. 4) Oblique photographs of each treeline type are presented in Fig. 5.

Above- and below-ground carbon storage across treelines

Across all treeline types mean SOC pools were 15.6 ± 1.4 kg C m^{-2} and carbon storage within above-ground biomass had a mean of 0.02 ± 0.01 kg C m^{-2} (Table 2). Mean SOC was significantly different ($p = 0.04$) across treeline types. Tukey HSD pairwise comparisons indicated that mean SOC was highest in MW sites (16.3 ± 0.8 kg C m^{-2}) compared to MT (15.8 ± 1.2 kg C m^{-2}; $p = 0.12$) and SW (14.5 ± 1.3 kg C m^{-2}; $p = 0.06$). Mean litter layer depths were significantly different ($p = 0.05$) among sites, and were highest in SW (0.8 cm ± 0.1) compared to MW site, (0.4 cm ± 0.1; $p = 0.06$) and MT (0.6 cm ± 0.1; $p = 0.13$). The C:N ratio was also significantly lower ($p = 0.001$) within MW, (20.3 ± 0.6) compared to MT (25.3 ± 1.1; $p = 0.005$). Mean soil C content (%), organic matter depth and bulk density did not differ significantly among treeline types.

Mean above-ground carbon storage did not differ among treeline types ($p = 0.1$), although carbon storage in above-ground tree biomass was higher ($p = 0.08$) in SW sites (0.04 kg m^{-2}) than MT sites (0.006 kg m^{-2}; $p = 0.08$). Across all sites, the majority (78%–98%) of carbon in above-ground biomass was stored in understory shrubs (Table 2). MW and SW had similar proportions of biomass stored in trees (25% and 18%, respectively) but MT sites had much less (5%). The allometric

Fig. 4. Cover of plant functional groups within 1 and 3 m^2 plots ($n = 55$) among the three treeline types (Moist Tundra, Mesic Woodland, and Submesic Woodland). Note that percent cover can exceed 100 as overlapping layers of plants within the same functional group were summed together.

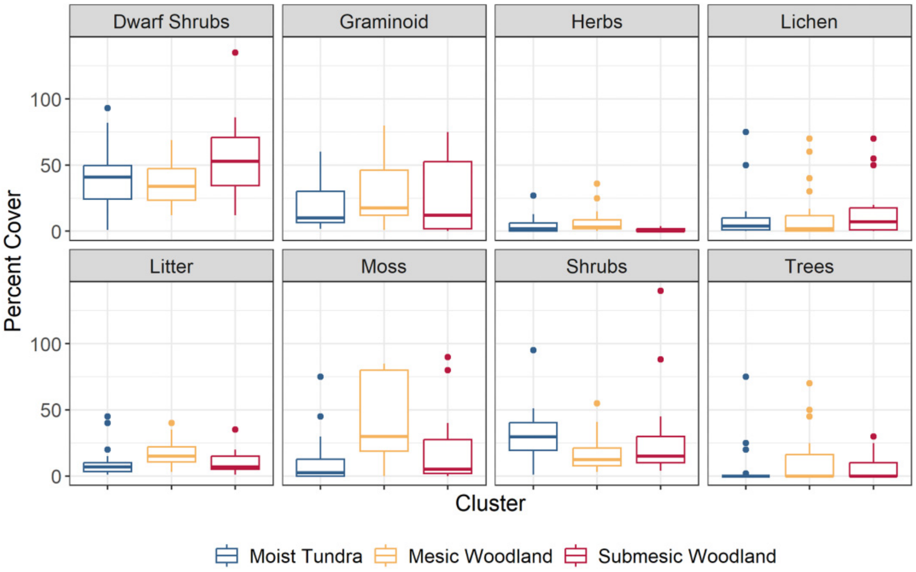

Fig. 5. Oblique imagery of the three treeline types. The yellow arrows show the approximate direction of transects across local treelines (note that the arrows do not show the exact location of the transects).

Cluster 1: Moist Tundra (MT)

Cluster 2: Mesic Woodland (MW)

Cluster 3: Submesic Woodland (SW)

model used to estimate tree biomass had an overall residual standard error of 8.62 kg.

For all soil samples, there were slight increases in SOC storage between samples with low and high stem density, but relatively little variation in SOC storage at higher stem densities (Fig. 6A). The range in SOC storage was greatest at low stem densities due in part to variation in organic soil depth (Fig. 6A). For all three treeline types median SOC storage increased slightly with stems per hectare and variation in SOC storage decreased with stem density (Fig. 6B).

Fine-scale drivers of soil carbon storage across the treeline

Ordinary least squares regression models indicate the relationship between SOC storage and fine-scale vegetation structure and microtopography differed among treeline types (Table 3). Mean vegetation height exhibited a significant positive relationship with SOC for MT sites ($p = 0.04$) and nonsignificant positive and negative relationships in MW sites (Fig. 7A), and SW sites, respectively. TPI showed a negative relationship ($p = 0.02$) with SOC in MT, indicating that topographic depressions had higher SOC. Terrain roughness also exhibited negative relationship with SOC in MW ($p = 0.01$) and nonsignificant relationships in MT sites, indicating that samples in areas with less topographic variation had higher SOC.

We also investigated drivers of bulk density, organic layer depth, and C content (%) individually (Table 3). Soil bulk density increased significantly with maximum vegetation height in the global model ($p = 0.04$) and with mean height in MW sites ($p < 0.001$; Fig. 7B). Slope was also a significant negative predictor of bulk density ($p = 0.003$) in MW sites, but was not significant in any other model. In MT and SW sites, vegetation height did not show significant relationships with bulk density. Organic layer depth did not show any significant relationships with vegetation structure or litter layer depth.

Fig. 6. Variation in soil organic carbon (SOC) storage (kg C m^{-2}) and tree stem density, calculated as the number of stems > 2.5 m within 30 m of each soil sample. Panel A shows SOC across all treeline types ($n = 140$); point color represents sample bulk density and size represents depth of the organic soil layer. The *y*-axis of Panel A has been logarithmically transformed. Panel B shows variation in SOC across four classes of increasing stem density within the three treeline types, as well as the median and Interquartile Range (IQR).

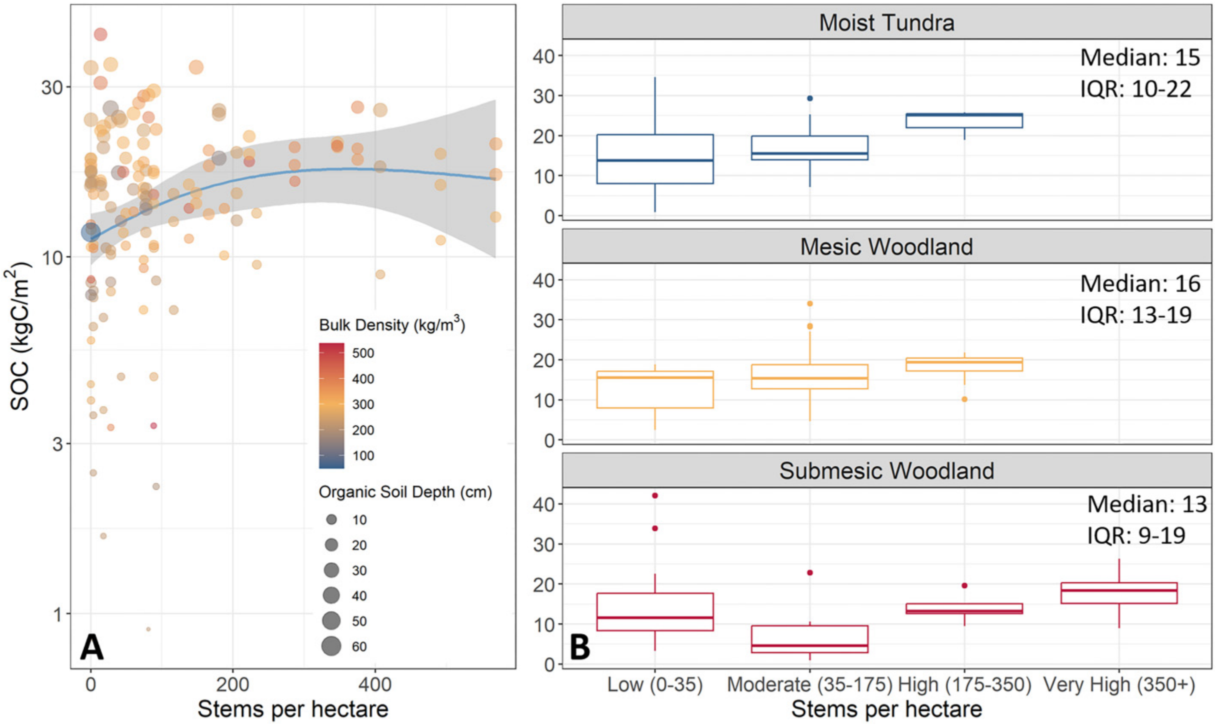

Surface roughness was a significant negative predictor of organic layer depth only in MW sites ($p = 0.02$).

Carbon content (%) decreased significantly with maximum height in the global model ($p = 0.005$) and for MW sites ($p = 0.02$; Fig. 7C). Maximum vegetation height was included in the final model for SW sites, but it was not statistically significant ($p = 0.13$; Table 3). Litter layer depth also had a positive relationship with carbon content in the global model ($p = 0.05$) and in MW areas ($p = 0.03$; Table 3). Topographic metrics including slope, aspect, and roughness were significant predictors of soil carbon content in the global model and within the SW and MT sites. Samples on south-facing ($p = 0.02$), steeper slopes ($p = 0.004$) exhibited higher carbon content in the global model. Roughness exhibited a strong positive relationship with carbon content in SW sites ($p = 0.002$); indicating that samples in areas with more varied terrain had higher carbon content.

Comparing drone vegetation metrics to Landsat spectral indices

Overall, Landsat indices at 30 m resolution showed linear and nonlinear relationships with the ExG index and tree stem counts derived from high-resolution drone surveys (Fig. 8). ExG showed a moderate positive relationship with Landsat EVI ($r^2 = 0.33$, RMSE: 18.19) and TCG ($r^2 = 0.31$, RMSE: 18.39), two measures linked to vegetation productivity. Landsat TCW showed the strongest positive associations with ExG ($r^2 = 0.54$; RMSE: 15.0). Canopy height and stem density showed weaker relationships with spectral indices with r^2 values ranging from 0.02 to 0.35. With the exception of TCW, all Landsat indices showed negative relationships with tree stem counts. TCB was the best predictor of tree stem count ($r^2 = 0.32$, RMSE: 7.03), with lower TCB associated with greater tree stem density. TCG was the best predictor of maximum canopy height ($r^2 = 0.35$, RMSE: 2.23) and all Landsat spectral indices exhibited negative relationships with canopy height.

Predicting treeline types

We predicted treeline type for 21 km of unsampled terrain across the study area. Of the 35 unsampled treelines sites, 17 (48%) were classified as MW, 12 (34%) were classified as MT, and 6 (18%) were classified as SW. Landscape types were spatially clustered, MT treelines are located in the southern margins of our study area while MW and SW treelines are concentrated at the northern end of the study area (Fig. 9). This distribution largely reflects landscape variation in elevation, surficial geology, and drainage. Treelines at the northern portion of the study area are generally located at higher elevation (Fig. 1) on well-drained sites underlain by till (Ecosystem Classification Group 2012). Across the southern portion of the study area, pond density and wetness increase within more hummocky lowlands (Fig. 1; Ecosystem Classification Group 2012).

Table 3. Regression coefficients and significance for all linear models ($p < 0.001 = ^{***}$, $p < 0.01 = ^{**}$, $p < 0.05 = ^{*}$, $p < 0.1 = ^{\wedge}$).

Model	Intercept	Log (mean height)	Log (max height)	Height SD	Litter layer	Log (rough)	Aspect	Slope	TPI
SOC (kg C m^{-2})									
Global	15.629	-	-	-	-	-	-	-	-
1. MT ($n = 46$)	29.716	2.402^{*}	-	-	-	3.845	-	-	-75.147^{*}
2. MW ($n = 59$)	9.043	$1.514^{\wedge}$	-	-	-	-4.571^{*}	-	-	-
3. SW ($n = 40$)	16.078	-	-	−1.947	-	-	-	-	-
Bulk density (kg m^{-3})									
Global	293.762	-	9.843^{*}	-	-18.784^{**}	-	-	-	-
1. MT ($n = 46$)	262.928	-	-	-	-	-	$0.184^{\wedge}$	-	-
2. MW ($n = 59$)	521.137	64.78^{***}	-	-84.968^{*}	-	-	-	-18.942^{**}	463.912
3. SW ($n = 40$)	304.783	-	-	-	$-20.933^{\wedge}$	-	-	-	-
Organic depth (cm)									
Global	15.082	-	-	-	-	-	-	-	−35.265
1. MT ($n = 46$)	30.549	-	-	-	-	$6.342^{\wedge}$	−0.025	-	-
2. MW ($n = 59$)	7.267	-	-	-	-	-3.296^{*}	-	-	-
3. SW ($n = 40$)	13.425	-	-	-	-	-	-	-	-
C content (%)									
Global	28.813	-	-0.808^{**}	-	$0.793^{\wedge}$	−2.233	-0.009^{*}	1.224^{**}	-
1. MT ($n = 46$)	33.066	-	-	-	-	$-2.132^{\wedge}$	-0.014^{*}	-	-
2. MW ($n = 59$)	35.591	-	-0.992^{*}	-	1.681^{*}	-	−0.008	-	-
3. SW ($n = 40$)	47.015	-	−0.859	-	-	4.566^{***}	-	-	-

Note: Models were fit using stepwise variable selection and only variables retained in the final model are shown in the table. Canopy height (mean, maximum, and standard deviation) was calculated from the drone-derived CHM. Litter layer depth was recorded in the field. Microtopographic variables (roughness, aspect, slope, Topographic Position Index) were calculated from the drone-derived DEM. TPI, Topographic Position Index; SOC, soil organic carbon; MT, Moist Tundra; MW, Mesic Woodland; SW, Submesic Woodland.

Discussion

In this analysis, we show associations between vegetation structure and below-ground carbon storage across three ecological treeline types underlain by continuous permafrost in the Northwest Territories, Canada. Consistent with previous studies (Wilmking et al. 2006; Siewert et al. 2015; Clemmensen et al. 2021), we observed that below-ground carbon pools were much larger than above-ground carbon pools. We also observed evidence of small increases in SOC stocks with increasing tree stem density and vegetation height across all treeline types. This is notably different from other observations across alpine treelines (Parker et al. 2015; Clemmensen et al. 2021; Kemppinen et al. 2021), or in discontinuous permafrost (Wilmking et al. 2006) where SOC stocks doubled between tundra and forest sites. Our findings suggest that potential losses of soil carbon in the upper organic horizon due to increasing forest and shrub density are mediated by the effects of microtopography, which can influence soil moisture and soil temperature at fine-spatial scales (Zona et al. 2011; Pichler et al. 2022). Instead, permafrost thaw and active layer deepening may be more significant drivers of soil carbon losses in this region relative to vegetation change (Kokelj et al. 2023). Additional studies throughout northwestern Canada and elsewhere should be conducted to confirm these observations, taking advantage of increasing coverage of drone imagery in various treeline environments (van der Sluijs et al. 2018; Orndahl et al. 2022).

Differences in soil carbon decomposition between treeline types

Rates of soil carbon decomposition and accumulation represented by C:N ratios and organic layer depths varied between the three treeline site types. Overall, the MT sites showed evidence of slower rates of decomposition and more soil carbon accumulation, while the woodland sites, MW, and SW, exhibited higher rates of decomposition and less carbon accumulation. MT sites had significantly higher C:N ratios as well as deeper organic layers compared to MW and SW sites (Table 2). More rapid decomposition at MW and SW sites can result from greater tree cover which is associated with higher ground temperatures and soil biological activity (Cleve et al. 1981). In the Tuktoyaktuk Coastlands, ground temperatures in upland forests are generally higher than tundra sites throughout the year, with the greatest difference observed over the winter (Palmer et al. 2012).

Despite evidence of more rapid decomposition and organic matter turnover within the woodland sites, there were relatively small differences in mean SOC storage between treeline types compared to previous studies (Parker et al. 2015; Clemmensen et al. 2021). This could reflect more gradual vegetation transitions in our study area, similarities in the cover of plant functional groups across transects (Fig. 4), or the presence of permafrost, which could decrease the effects of plant communities on soil C storage (Hartley et al. 2012; Wagner et al. 2023). However, small changes in mean SOC

Fig. 7. Linear relationships between soil bulk density and soil organic carbon (SOC) in relation to vegetation structure metrics among treeline types. They greyscale plots indicate when a predictor variable was not included in the final linear model after stepwise variable selection.

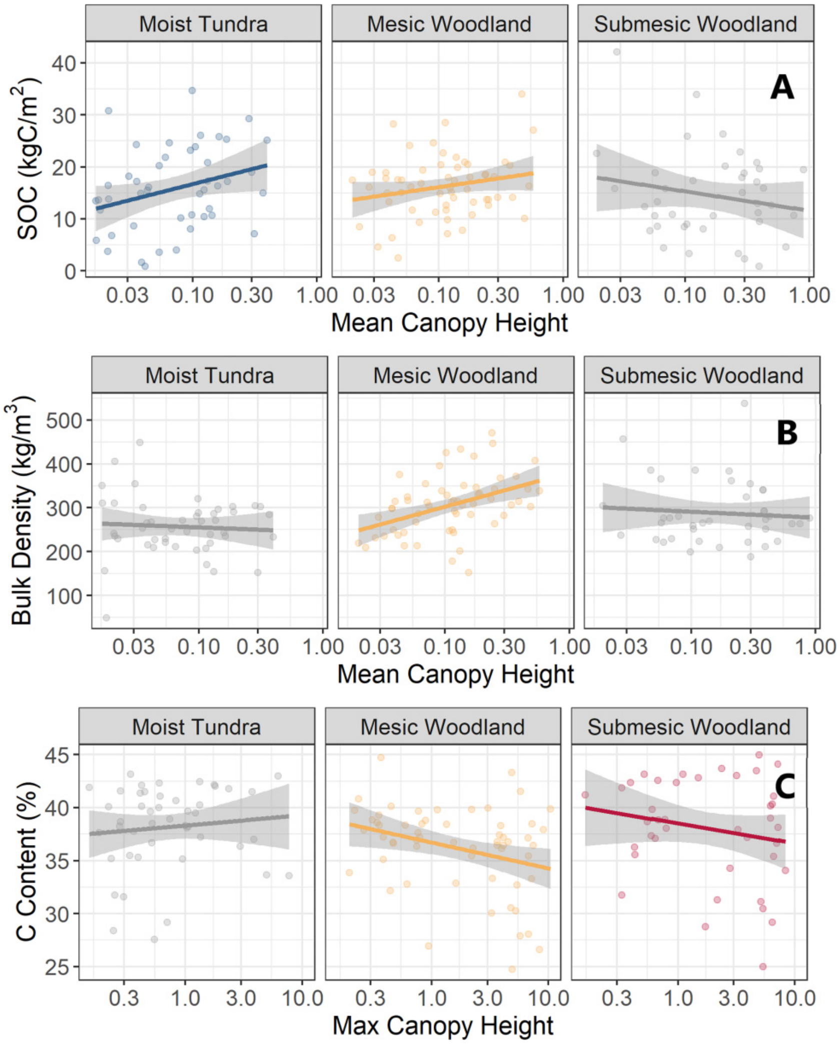

storage could still result in significant carbon losses to the atmosphere if these changes are consistent over large areas (Parker et al. 2021). Larger differences in SOC storage may be observed by comparing tundra sites to more densely treed boreal sites below the treeline, however, our treeline transects were selected to reflect anticipated changes in stem density across tree and shrublines occurring over annual or decadal scales. Future work should also consider the placement of treeline transects to capture potential effects of range expansion on SOC storage. Our experimental design was intended to capture changes in SOC from unforested to sparsely forested woodlands synonymous to increasing stem density at local scales. The transects do not necessarily reflect changes related to species or biome-scale range shifts, especially given that spruce trees in this area limited reproduction at the northern margins of their range (Lantz et al. 2019; Travers-Smith and Lantz 2020).

Overall, MW sites stored the most SOC (16.3 kg C m^{-2}), and SW stored the least (14.5 kg C m^{-2}) and MT was intermediate (15.8 kg C m^{-2}). This could reflect differences in understory community composition as well as site topography, which can influence important controls such as soil moisture and nutrient accumulation. The SW sites showed the greatest topographic variation and the smallest SOC stocks, reflecting sites on well-drained slopes, and ridges with drier and warmer soils (Wojcik et al. 2019). Given the association with topography, soil moisture and organic soil thickness, future SOC upscaling work should emphasize abiotic factors such as landform classifications (Wojcik et al. 2019), surficial geology (Rampton 1988), and permafrost features (Robinson and Moore 2000; Siewert et al. 2015;) to expand on the SOC associations observed in this study.

Increases in SOC stocks with increasing stem density

At the MT and MW sites we observed slight increases in SOC storage with increasing tree stem density and

Fig. 8. Relationships between Landsat spectral indices (Enhanced Vegetation Index, Tasseled Cap Brightness, Greenness and Wetness) with drone metrics (Excess Greenness, per pixel tree stem counts, and maximum canopy height). RMSE and r^2 values are extracted from Generalized Additive Models. Red plots show the best single Landsat spectral index to predicts each drone variable. EVI, Enhanced Vegetation Index; TCB, Tasseled Cap Brightness; TCG, Tasseled Cap Greenness; TCW, Tasseled Cap Wetness; RMSE, room mean square error.

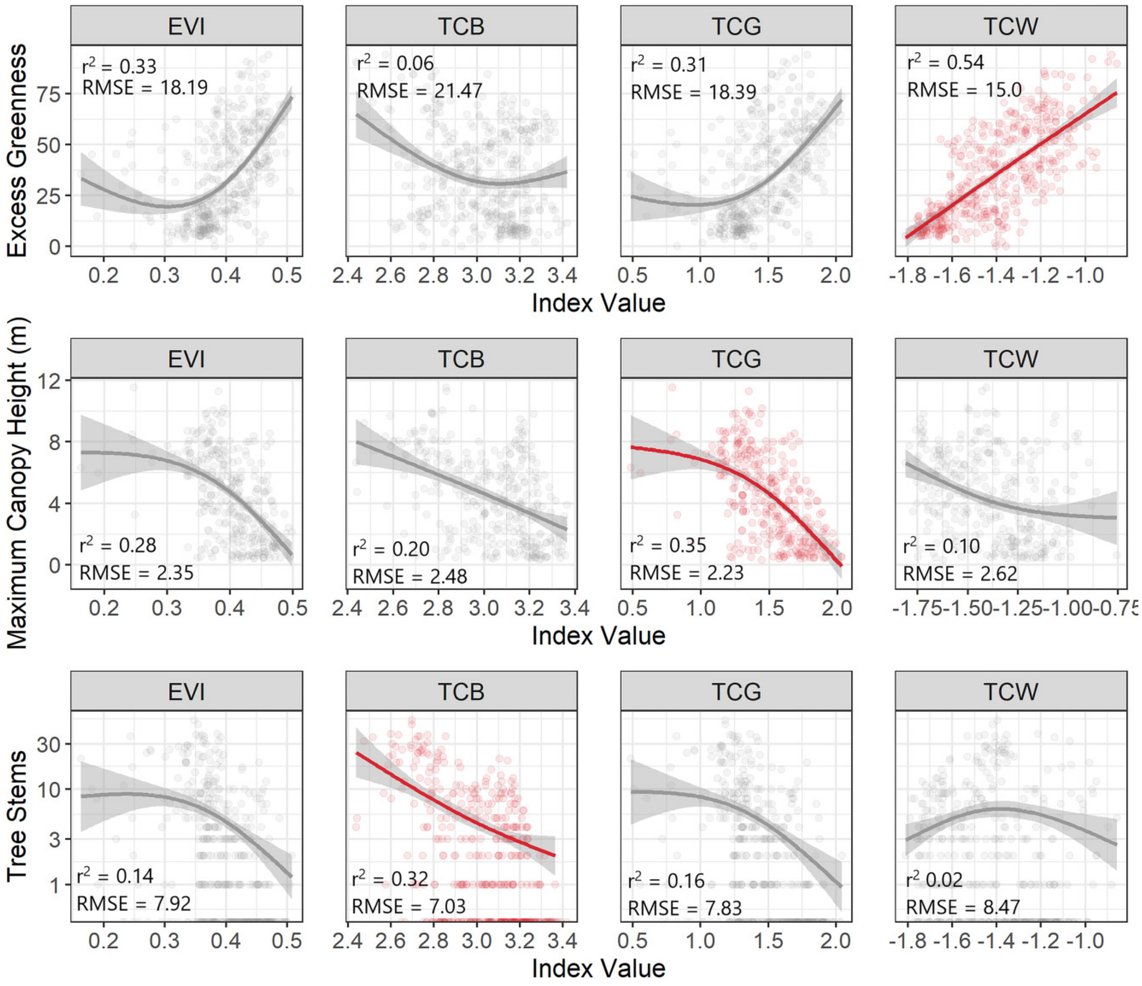

vegetation height (Figs. 6 and 7). These findings are consistent with Devos et al. (2022) who reported greater median SOC storage in forest soils compared to tundra soils at 14 treeline sites across Norway. We also observed that when stem density was low, there was larger variation in SOC stocks due to variability in the soil organic layer depth. This suggests that topographic factors that influence organic layer depth may mediate the effects of vegetation communities on SOC stocks across the treeline, particularly at sites with low tree density. In MT sites, SOC storage increased with mean canopy height, but bulk density, carbon content, and organic matter depth did not show strong relationships with vegetation height. Instead, microtopography including surface roughness and aspect were more significant predictors of soil characteristics. Soil moisture and temperature, in part controlled by topographic factors such as aspect and surface roughness (Cleve et al. 1981), are likely influencing both soil carbon accumulation and vegetation structure across our treeline sites (Rodionov et al. 2007; Zona et al. 2011). Our results suggest that abiotic factors controlling soil temperature and moisture may limit the effects of tree density and vegetation growth on SOC stocks.

At MW sites we observed strong increases in bulk density with increasing canopy height that resulted in increasing SOC storage across the treeline and greater SOC storage compared to other site types. Higher soil bulk density has been associated with warmer, more compacted soils, increased nutrient mineralization, and plant productivity (Chapin and Shaver 1981), as well as lower overall SOC content (%) and SOC storage (Bockheim et al. 2003). However, across the treeline types sampled here, differences in carbon content was relatively small (5% maximum difference between treeline types), compared to differences in bulk density (20% maximum difference; Table 3). Thus, bulk density had a greater influence on overall SOC storage within MW sites compared to organic matter depth and carbon content (%). These results suggest that the relative influence of soil structural properties (density) and biological activity

Fig. 9. Map showing the distribution of predicted treeline types at 200 m intervals ($n = 35$) along all localized treelines within the study area. The solid lines show the mapped treelines and the points indicate the treeline type, which were classified using topographic and spectral indices for transects crossing the treeline.

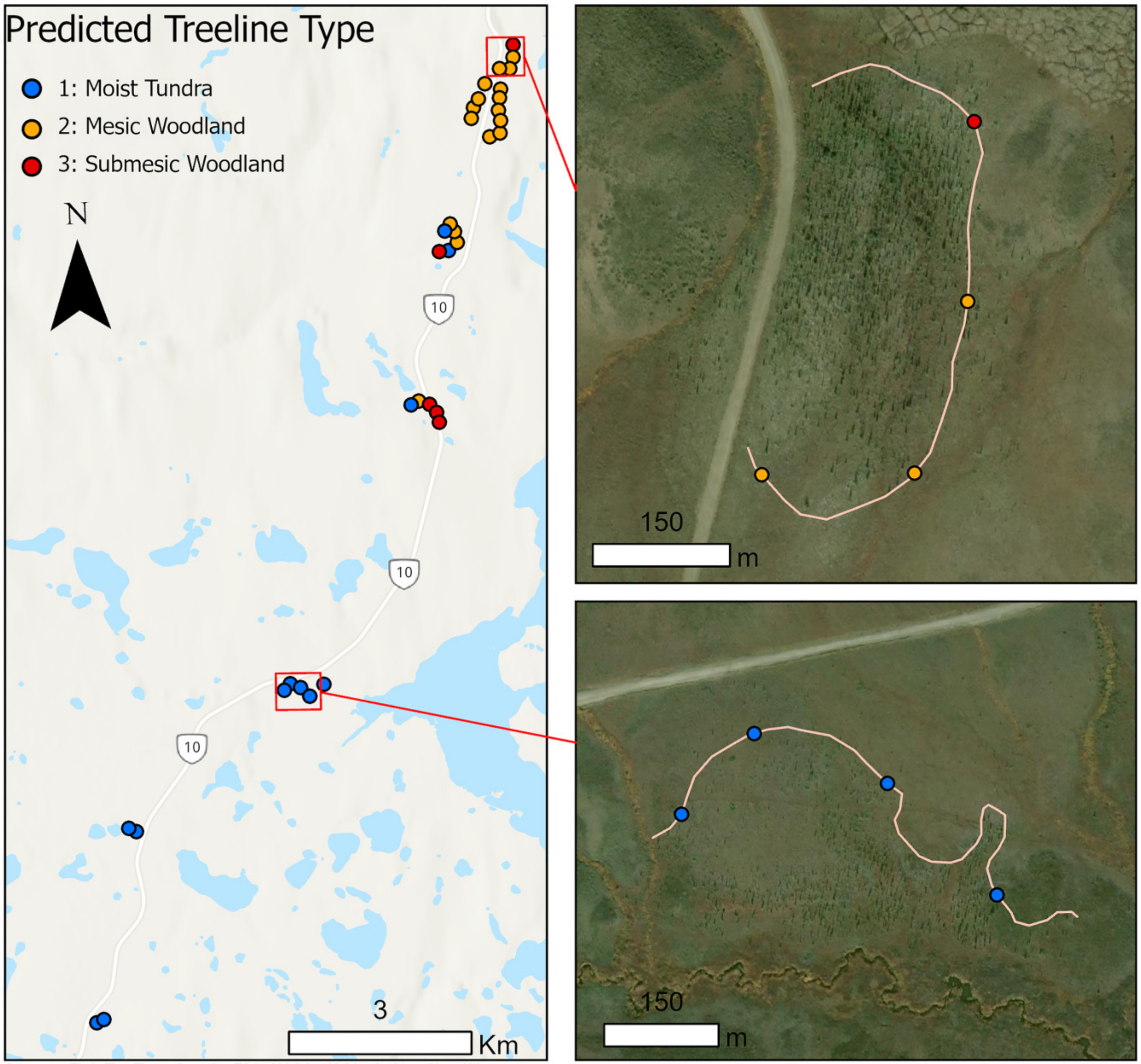

Sources: Esri, TomTom, Garmin, FAO, NOAA, USGS, © OpenStreetMap contributors, and the GIS User Community, Esri, USGS, Maxar

(carbon content) on SOC storage may vary among different site types.

Multiple Landsat indices reflect variation in forest structure at the treeline

Comparisons of Landsat 30 m spectral indices with drone imagery show that spectral indices can capture fine-scale changes in site productivity and forest structure at the treeline, particularly for indices that utilize the short-wave infrared bands, such as TCB and TCW. These findings align with recent Landsat-based efforts to produce detailed forest inventories of northern boreal forests in the Northwest Territories (Castilla et al. 2022; van der Sluijs et al. 2023*a*). Drone-derived ExG estimates were moderately correlated with increasing spectral greenness represented by the EVI ($r^2 = 0.33$) and TCG ($r^2 = 0.31$) from Landsat (Richardson et al. 2007). However, TCW showed a stronger positive correlation ($r^2 = 0.54$) with ExG compared to EVI and TCG. The stronger correlations of ExG and TCW likely reflects the ability of ExG to capture leaf area and vegetation composition (Kauth and Thomas 1976). EVI and TCG were highest within the MT sites, likely reflecting the relatively high alder and willow cover at these sites (29.5%).

Tree stem density and maximum canopy height showed negative relationships with Landsat spectral indices (Fig. 8). Notably, TCB exhibited the strongest decrease with increasing tree density ($r^2 = 0.32$, Fig. 8) and TCG also decreased with increasing maximum vegetation height ($r^2 = 0.35$). These results are likely driven by the influence of shadows and woody stems in higher density stands, which are expected to affect spectral mixtures and decrease overall reflectance (Fraser et al. 2014*b*; Pickell et al. 2016; van der Sluijs et al. 2023*a*). Lower spectral greenness at more densely forested sites may also reflect greater moss and lichen cover in the understory, which can increase brightness and decrease greenness (Fraser et al. 2014*b*; Fig. 4). These findings support previous work in the forest-tundra ecotone that highlight poor correspondence between fine-scale forest structure and medium resolution (30 m) spectral greenness data due to confounding impacts of upright shrubs and understory vegetation (Timoney and Mamet 2020). Taken together, this indicates that widespread spectral greening is not indicative of increases in forest cover, or density and treeline expansion in sparsely treed areas (Loranty et al. 2018; Berner and Goetz 2021; Walker et al. 2021).

Extending measures of soil characteristics with remote sensing

Although spectral reflectance is not inherently sensitive to below-ground phenomenon, in our analysis we were able to link distinct spectral signatures to landscape types representing differences in above- and belowground carbon storage. Predicting the frequency of these treeline types across our study area shows that the most commonly occurring type was MW, representing 48% of treeline sites. These sites were concentrated along the northern margin of our study area within higher elevation uplands (Fig. 9; Ecosystem Classification Group 2012). MT site types were predicted at 34% of treelines and were located in the southern half of the study area. This region is typified by lower lying sites with complex drainage patterns between many small streams and waterbodies (Ecosystem Classification Group 2012). Both the MW and MT sites showed small increases in SOC storage with increasing vegetation height and tree stem density. This finding suggests that for the majority of our study area, vegetation growth across tree and shrublines in low-relief areas may not trigger large losses of SOC storage. Only the sloped SW sites (18% of the predicted treeline types) showed a nonsignificant decrease in SOC with vegetation height.

These results suggest that landscape position and broad-scale drainage characteristics are important considerations when scaling estimates of SOC storage at the treeline. However, a large range in SOC within site types highlights significant challenges in directly predicting SOC with medium resolution satellite data such as Landsat, which has 900 m^2 pixel area. Improvements in SOC estimation through remote sensing may also be achieved using different statistical techniques (e.g., partial least square regression), machine learning in combination with higher spatial resolution spectral data or sensors that capture variation in soil properties below the vegetation canopy (e.g., radar).

Soil sampling limitations and future directions

To improve monitoring of SOC stocks at the northern treeline, future studies should consider changes in both organic and mineral pools as well as variation at different depths within each horizon. Following similar studies conducted across northern treelines (Parker et al. 2015; Devos et al. 2022) and shrublines (Kemppinen et al. 2021), we focused our soil analysis on homogenized samples of the unfrozen organic horizon. However, analyses of SOC stocks in the boreal (Walker et al. 2020; Bill et al. 2023) and tundra (Wagner et al. 2023) have shown that bulk density and carbon content varies within 5–100 cm of the soil profile. In this analysis we assumed that interactions between vegetation and soil carbon stocks were present within the organic horizon—but it is possible that variation in vegetation structure impacted SOC stocks deeper in the mineral horizon as well (Mack et al. 2004; Street et al. 2020).

Conclusions

In this study, we mapped above-ground biomass and sampled carbon stored in the surface organic layer across latitudinal treelines in the Northwest Territories, Canada. Despite higher rates of organic matter decomposition within tundra sites, we observed small overall increases in SOC with increasing vegetation height and tree stem density. Our results suggest that microtopography as well as broad scale landscape position and drainage patterns influencing soil temperature and moisture, may be stronger drivers of soil carbon storage than vegetation structure in regions underlain by continuous permafrost. Our work also underscores the value of utilizing remote sensing data at various scales for enhancing fine-scale mapping of vegetation structure and terrain characteristics, which can provide insight into the spatial distribution of below-ground carbon storage.

Acknowledgements

The authors would like to express gratitude to the Inuvialuit for allowing this research to be conducted on their land. Field work was conducted within the Inuvialuit Settlement Region under a Scientific Research License granted to Trevor Lantz (License Number: 17296). This work was funded in part through the Canadian Space Agency (Grant number: 21SUESECDL) and by NSERC support of Nicholas Coops (RGPIN-2018-03851) and Trevor Lantz (RGPIN 2018-06210). We also acknowledge funding support to Hana Travers-Smith from the NSERC Canada Graduate Scholarship-Doctoral and the University of British Columbia. Thank you to Trevor Lantz and members of the Arctic Landscape Ecology Lab, Meghan Hamp, and Hayley Webster who assisted with field data collection.

Article information

History dates

Received: 18 June 2024
Accepted: 14 December 2024
Accepted manuscript online: 20 December 2024
Version of record online: 3 February 2025

Copyright

Data availability

SOC and plot data and R code supporting this work are publicly available in the GitHub repository, https://github.com/hztraver/SOC_Modeling. Additional code, data, and model outputs are available upon request from the authors.

Author information

Author ORCIDs

H. Travers-Smith https://orcid.org/0000-0002-9338-0633
T.C. Lantz https://orcid.org/0000-0001-5643-1537
J. van der Sluijs https://orcid.org/0000-0002-9244-1756

Author contributions

Conceptualization: HT, NCC, TCL
Data curation: JvdS
Formal analysis: HT
Funding acquisition: NCC
Investigation: HT
Methodology: HT, TCL, MH
Supervision: NCC, TCL, DI, MAW
Visualization: HT
Writing – original draft: HT
Writing – review & editing: NCC, TCL, MH, DI, MAW, JvdS

Competing interests

The authors declare there are no competing interests.

Supplementary material

Supplementary data are available with the article at https://doi.org/10.1139/as-2024-0048.

References

Berner, L.T., and Goetz, S.J. 2022. Satellite observations document trends consistent with a boreal forest biome shift. Global Change Biology, **28**: 3275–3292. doi:10.1111/gcb.16121.

Bill, K.E., Dieleman, C.M., Baltzer, J.L., Degré-Timmons, G.É., Mack, M.C., Day, N.J., et al. 2023. Post-fire recovery of soil organic layer carbon in Canadian boreal forests. Ecosystems, **26**: 1623–1639. doi:10.1007/s10021-023-00854-0.

Bockheim, J.G., Hinkel, K.M., and Nelson, F.E. 2003. Predicting carbon storage in Tundra soils of arctic Alaska. Soil Science Society of America Journal, **67**: 948–950. doi:10.2136/sssaj2003.9480.

Castilla, G., Hall, R.J., Skakun, R., Filiatrault, M., Beaudoin, A., Gartrell, M., et al. 2022. The multisource vegetation Inventory (MVI): a satellite-based forest inventory for the Northwest Territories Taiga Plains. Remote Sensing, **14**: 1108. doi:10.3390/rs14051108.

Chapin, F.S., and Shaver, G.R. 1981. Changes in soil properties and vegetation following disturbance of Alaskan Arctic Tundra. The Journal of Applied Ecology, **18**: 605–617. doi:10.2307/2402420.

Clemmensen, K.E., Durling, M.B., Michelsen, A., Hallin, S., Finlay, R.D., and Lindahl, B.D. 2021. A tipping point in carbon storage when forest expands into tundra is related to mycorrhizal recycling of nitrogen. Ecology Letters, **24**: 1193–1204. doi:10.1111/ele.13735.

Clemmensen, K.E., Finlay, R.D., Dahlberg, A., Stenlid, J., Wardle, D.A., and Lindahl, B.D. 2015. Carbon sequestration is related to mycorrhizal fungal community shifts during long-term succession in boreal forests. New Phytologist, **205**: 1525–1536. doi:10.1111/nph.13208.

Cleve, K.V., Barney, R., and Schlentner, R. 1981. Evidence of temperature control of production and nutrient cycling in two interior Alaska black spruce ecosystems. Canadian Journal of Forest Research, **11**: 259–274. doi:10.1139/x81-035.

Cornelissen, J.H.C., Van Bodegom, P.M., Aerts, R., Callaghan, T.V., Van Logtestijn, R.S.P., Alatalo, J., et al. 2007. Global negative vegetation feedback to climate warming responses of leaf litter decomposition rates in cold biomes. Ecology Letters, **10**: 619–627. doi:10.1111/j.1461-0248.2007.01051.x.

Devos, C.C., Ohlson, M., Næsset, E., and Bollandsås, O.M. 2022. Soil carbon stocks in forest-tundra ecotones along a 500 km latitudinal gradient in northern Norway. Scientific Reports, **12**: 13358. doi:10.1038/s41598-022-17409-3.

Ecosystem Classification Group. 2012. Ecological regions of the northwest territories—Southern Arctic (No. x + 170 pp. + insert map). Department of Environment and Natural Resources, Government of the Northwest Territories, Yellowknife, NT, Canada.

Environment and Climate Change Canada [ECCC]. 2024. National Climate Data and Historical Information Archive. https://climate.weather.gc.ca/historical_data.

Flade, L., Hopkinson, C., and Chasmer, L. 2020. Allometric equations for shrub and short-stature tree aboveground biomass within boreal ecosystems of Northwestern Canada. Forests, **11**: 1207. doi:10.3390/f11111207.

Fraser, R.H., Lantz, T.C., Olthof, I., Kokelj, S.V., and Sims, R.A. 2014a. Warming-induced shrub expansion and lichen decline in the western Canadian arctic. Ecosystems, **17**: 1151–1168. doi:10.1007/s10021-014-9783-3.

Fraser, R.H., Olthof, I., Kokelj, S.V., Lantz, T.C., Lacelle, D., Brooker, A., et al. 2014b. Detecting landscape changes in high latitude environments using Landsat trend analysis: 1. Visualization. Remote Sensing, **6**: 11533–11557. doi:10.3390/rs61111533.

Fraser, R.H., Olthof, I., Lantz, T.C., and Schmitt, C. 2016. UAV photogrammetry for mapping vegetation in the low-Arctic. Arctic Science, **2**: 79–102. doi:10.1139/as-2016-0008.

Fraser, R.H., van der Sluijs, J., and Hall, R.J. 2017. Calibrating satellite-based indices of burn severity from UAV-derived metrics of a burned boreal forest in NWT, Canada. Remote Sensing, **9**: 279. doi:10.3390/rs9030279.

Gill, H.K., Lantz, T.C., O'Neill, B., and Kokelj, S.V. 2014. Cumulative impacts and feedbacks of a gravel road on shrub tundra ecosystems in the Peel Plateau, Northwest Territories, Canada. Arctic, Antarctic, and Alpine Research, **46**: 947–961. doi:10.1657/1938-4246-46.4.947.

Greaves, H.E., Vierling, L.A., Eitel, J.U.H., Boelman, N.T., Magney, T.S., Prager, C.M., and Griffin, K.L. 2017. Applying terrestrial lidar for evaluation and calibration of airborne lidar-derived shrub biomass estimates in Arctic tundra. Remote Sensing Letters, **8**: 175–184. doi:10.1080/2150704X.2016.1246770.

Hammar, J., Grünberg, I., Kokelj, S.V., van der Sluijs, J., and Boike, J. 2023. Snow accumulation, albedo and melt patterns following road construction on permafrost, Inuvik–Tuktoyaktuk Highway, Canada. The Cryosphere, **17**: 5357–5372. doi:10.5194/tc-17-5357-2023.

Hansson, A., Dargusch, P., and Shulmeister, J. 2021. A review of modern treeline migration, the factors controlling it and the implications for carbon storage. Journal of Mountain Science, **18**: 291–306. doi:10.1007/s11629-020-6221-1.

Hartigan, J.A., and Wong, M.A. 1979. Algorithm AS 136: a K-means clustering algorithm. Applied Statistics, **28**: 100–108. doi:10.2307/2346830.

Hartley, I.P., Garnett, M.H., Sommerkorn, M., Hopkins, D.W., Fletcher, B.J., Sloan, V.L., et al. 2012. A potential loss of carbon associated with greater plant growth in the European Arctic. Nature Climate Change, **2**: 875–879. doi:10.1038/nclimate1575.

Hermosilla, T., Wulder, M.A., White, J.C., and Coops, N.C. 2022. Land cover classification in an era of big and open data: optimizing localized implementation and training data selection to improve mapping outcomes. Remote Sensing of Environment, **268**: 112780. doi:10.1016/j.rse.2021.112780.

Hermosilla, T., Wulder, M.A., White, J.C., Coops, N.C., and Hobart, G.W. 2015. An integrated Landsat time series protocol for change detection and generation of annual gap-free surface reflectance composites. Remote Sensing of Environment, **158**: 220–234. doi:10.1016/j.rse.2014.11.005.

Hijmans, R.J. 2022. raster: geographic data analysis and modeling.

Kassambara, A., and Mundt, F. 2020. factoextra: extract and visualize the results of multivariate data analyses.

Kauth, R.J., and Thomas, G.S. 1976. The tasselled cap—a graphic description of the spectral-temporal development of agricultural crops as seen by LANDSAT. LARS Symp. Paper 159.

Kemppinen, J., Niittynen, P., Virkkala, A.-M., Happonen, K., Riihimäki, H., Aalto, J., and Luoto, M. 2021. Dwarf shrubs impact tundra soils: drier, colder, and less organic carbon. Ecosystems, **24**: 1378–1392. doi:10.1007/s10021-020-00589-2.

Kokelj, S.V., Burn, C.R., and Tarnocai, C. 2007. The structure and dynamics of earth hummocks in the subarctic forest near Inuvik, Northwest Territories, Canada. Arctic, Antarctic, and Alpine Research, **39**: 99–109. doi:10.1657/1523-0430(2007)39[99:TSADOE]2.0.CO;2.

Kokelj, S.V., Gingras-Hill, T., Daly, S.V., Morse, P.D., Wolfe, S.A., Rudy, A.C.A., et al. 2023. The northwest territories thermokarst mapping collective: a northern-driven mapping collaborative toward understanding the effects of permafrost thaw. Arctic Science, **9**: 886–918. doi:10.1139/as-2023-0009.

Lantz, T.C., Gergel, S.E., and Henry, G.H.R. 2010. Response of green alder (Alnus viridis subsp. fruticosa) patch dynamics and plant community composition to fire and regional temperature in northwestern Canada. Journal of Biogeography, **37**: 1597–1610. doi:10.1111/j.1365-2699.2010.02317.x.

Lantz, T.C., Moffat, N.D., Fraser, R.H., and Walker, X. 2019. Reproductive limitation mediates the response of white spruce (*Picea glauca*) to climate warming across the forest–tundra ecotone. Arctic Science, **5**: 167–184. doi:10.1139/as-2018-0012.

Loranty, M., Davydov, S., Kropp, H., Alexander, H., Mack, M., Natali, S., and Zimov, N. 2018. Vegetation indices do not capture forest cover variation in Upland Siberian larch forests. Remote Sensing, **10**: 1686. doi:10.3390/rs10111686.

Mack, M.C., Schuur, E.A.G., Bret-Harte, M.S., Shaver, G.R., and Chapin, F.S. 2004. Ecosystem carbon storage in arctic tundra reduced by long-term nutrient fertilization. Nature, **431**: 440–443. doi:10.1038/nature02887. PMID: 15386009.

Maechler, M., Rousseeuw, P., Struyf, A., Hubert, M., and Hornik, K. 2022. Cluster: cluster analysis basics and extensions.

McGuire, A.D., Christensen, T.R., Hayes, D., Heroult, A., Euskirchen, E., Kimball, J.S., et al. 2012. An assessment of the carbon balance of Arctic tundra: comparisons among observations, process models, and atmospheric inversions. Biogeosciences, **9**: 3185–3204. doi:10.5194/bg-9-3185-2012.

Miner, K.R., Turetsky, M.R., Malina, E., Bartsch, A., Tamminen, J., McGuire, A.D., et al. 2022. Permafrost carbon emissions in a changing Arctic. Nature Reviews Earth & Environment, **3**: 55–67. doi:10.1038/s43017-021-00230-3.

Moffat, N.D., Lantz, T.C., Fraser, R.H., and Olthof, I. 2016. Recent vegetation change (1980–2013) in the Tundra ecosystems of the Tuktoyaktuk Coastlands, NWT, Canada. Arctic, Antarctic, and Alpine Research, **48**: 581–597. doi:10.1657/AAAR0015-063.

Montesano, P.M., Neigh, C.S.R., Macander, M., Feng, M., and Noojipady, P. 2020. The bioclimatic extent and pattern of the cold edge of the boreal forest: the circumpolar taiga-tundra ecotone. Environmental Research Letters, **15**: 105019. doi:10.1088/1748-9326/abb2c7.

Myers-Smith, I.H., and Hik, D.S. 2018. Climate warming as a driver of tundra shrubline advance. Journal of Ecology, **106**: 547–560. doi:10.1111/1365-2745.12817.

Orndahl, K.M., Macander, M.J., Berner, L.T., and Goetz, S. 2022. Plant functional type aboveground biomass change within Alaska and northwest Canada mapped using a 35-year satellite time series from 1985-2020. Environmental Research Letters, **17**: 115010. doi:10.1088/1748-9326/ac9d50.

Palmer, M.J., Burn, C.R., and Kokelj, S.V. 2012. Factors influencing permafrost temperatures across tree line in the uplands east of the Mackenzie Delta, 2004–2010. Canadian Journal of Earth Sciences, **49**(8): 877–894. doi:10.1139/e2012-002.

Parker, T.C., Subke, J.-A., and Wookey, P.A. 2015. Rapid carbon turnover beneath shrub and tree vegetation is associated with low soil carbon stocks at a subarctic treeline. Global Change Biology, **21**: 2070–2081. doi:10.1111/gcb.12793.

Parker, T.C., Thurston, A.M., Raundrup, K., Subke, J.-A., Wookey, P.A., and Hartley, I.P. 2021. Shrub expansion in the Arctic may induce large-scale carbon losses due to changes in plant-soil interactions. Plant and Soil, **463**: 643–651. doi:10.1007/s11104-021-04919-8.

Pichler, V., Gömöryová, E., Merganič, J., Fleischer, P., Homolák, M., Onuchin, A., et al. 2022. Interrelationships among mountain relief, surface organic layer, soil organic carbon, and its mineral association under subarctic forest tundra. Scientific Reports, **12**: 17252. doi:10.1038/s41598-022-21521-9.

Pickell, P.D., Hermosilla, T., Frazier, R.J., Coops, N.C., and Wulder, M.A. 2016. Forest recovery trends derived from Landsat time series for North American boreal forests. International Journal of Remote Sensing, **37**: 138–149. doi:10.1080/2150704X.2015.1126375.

R Core Team. 2022. R: a language and environment for statistical computing. R Foundation for Statistical Computing, Vienna, Austria.

Rampton, V.N. 1988. Quaternary geology of the Tuktoyaktuk Coastlands, Northwest Territories., Geological Survey of Canada (No. Memoir 423). Ottawa, ON.

Richardson, A.D., Jenkins, J.P., Braswell, B.H., Hollinger, D.Y., Ollinger, S.V., and Smith, M.-L. 2007. Use of digital webcam images to track spring green-up in a deciduous broadleaf forest. Oecologia, **152**: 323–334. doi:10.1007/s00442-006-0657-z. PMID: 17342508.

Robinson, S.D., and Moore, T.R. 2000. The influence of permafrost and fire upon carbon accumulation in high boreal peatlands, Northwest Territories, Canada. Arctic, Antarctic, and Alpine Research, **32**: 155–166. doi:10.2307/1552447.

Rodionov, A., Flessa, H., Grabe, M., Kazansky, O.A., Shibistova, O., and Guggenberger, G. 2007. Organic carbon and total nitrogen variability in permafrost-affected soils in a forest tundra ecotone. European Journal of Soil Science, **58**: 1260–1272. doi:10.1111/j.1365-2389.2007.00919.x.

Roussel, J.-R., Auty, D., Coops, N.C., Tompalski, P., Goodbody, T.R.H., Meador, A.S., et al. 2020. lidR: an R package for analysis of Airborne Laser Scanning (ALS) data. Remote Sensing of Environment, **251**: 112061. doi:10.1016/j.rse.2020.112061.

Siewert, M.B., Hanisch, J., Weiss, N., Kuhry, P., Maximov, T.C., and Hugelius, G. 2015. Comparing carbon storage of Siberian tundra and taiga permafrost ecosystems at very high spatial resolution. Journal of Geophysical Research: Biogeosciences, **120**: 1973–1994. doi:10.1002/2015JG002999.

Sistla, S.A., Moore, J.C., Simpson, R.T., Gough, L., Shaver, G.R., and Schimel, J.P. 2013. Long-term warming restructures Arctic tundra without changing net soil carbon storage. Nature, **497**: 615–618. doi:10.1038/nature12129. PMID: 23676669.

Sørensen, M.V., Strimbeck, R., Nystuen, K.O., Kapas, R.E., Enquist, B.J., and Graae, B.J. 2018. Draining the pool? Carbon storage and fluxes in three alpine plant communities. Ecosystems, **21**: 316–330. doi:10.1007/s10021-017-0158-4.

Storey, J., Choate, M., and Lee, K. 2014. Landsat 8 operational land imager on-orbit geometric calibration and performance. Remote Sensing, **6**: 11127–11152. doi:10.3390/rs61111127.

Street, L.E., Garnett, M.H., Subke, J.-A., Baxter, R., Dean, J.F., and Wookey, P.A. 2020. Plant carbon allocation drives turnover of old soil organic matter in permafrost tundra soils. Global Change Biology, **26**: 4559–4571. doi:10.1111/gcb.15134.

Tarnocai, C., Canadell, J.G., Schuur, E.A.G., Kuhry, P., Mazhitova, G., and Zimov, S. 2009. Soil organic carbon pools in the northern circumpolar permafrost region. Global Biogeochemical Cycles, **23**. doi:10.1029/2008GB003327.

Thomas, M., Monhonval, A., Hirst, C., Bröder, L., Zolkos, S., Vonk, J.E., et al. 2023. Evidence for preservation of organic carbon interacting with iron in material displaced from retrogressive thaw slumps: case study in Peel Plateau, western Canadian Arctic. Geoderma, **433**: 116443. doi:10.1016/j.geoderma.2023.116443.

Timoney, K.P., and Mamet, S. 2020. No treeline advance over the last 50 years in subarctic western and central Canada and the problem of vegetation misclassification in remotely sensed data. Écoscience, **27**: 93–106. doi:10.1080/11956860.2019.1698258.

Timoney, K.P., La Roi, G.H., Zoltai, S.C., and Robinson, A.L. 1992. The high subarctic forest-Tundra of Northwestern Canada: position, width, and vegetation gradients in relation to climate. Arctic, **45**: 1–9. doi:10.14430/arctic1367.

Travers-Smith, H.Z., and Lantz, T.C. 2020. Leading-edge disequilibrium in alder and spruce populations across the forest–tundra ecotone. Ecosphere, **11**: e03118. doi:10.1002/ecs2.3118.

Ung, C.-H., Lambert, M.C., Raulier, F., Guo, J., and Bernier, P.Y. 2017. Biomass of trees sampled across Canada as part of the

Energy from the Forest Biomass (ENFOR) Program. doi:10.23687/fbad665e-8ac9-4635-9f84-e4fd53a6253c.

van der Sluijs, J., Kokelj, S.V., Fraser, R.H., Tunnicliffe, J., and Lacelle, D. 2018. Permafrost terrain dynamics and infrastructure impacts revealed by UAV photogrammetry and thermal imaging. Remote Sensing, **10**: 1734. doi:10.3390/rs10111734.

van der Sluijs, J., Peddle, D.R., and Hall, R.J. 2023a. Characterizing tree species in Northern Boreal Forests using multiple-endmember spectral mixture analysis and multi-temporal satellite imagery. Canadian Journal of Remote Sensing, **49**: 2216312. doi:10.1080/07038992.2023.2216312.

van der Sluijs, J., Saiet, E., Bakelaar, C.N., Wentworth, A., Fraser, R.H., and Kokelj, S.V. 2023b. Beyond visual-line-of-sight (BVLOS) drone operations for environmental and infrastructure monitoring: a case study in northwestern Canada. Drone Systems and Applications, **11**: 1–15. doi:10.1139/dsa-2023-0012.

van der Sluijs, J., Saiet, E., Fraser, R.H., Kokelj, S.V., and Bakelaar, C.N. 2024. Validation of beyond visual-line-of-sight drone photogrammetry for terrain and canopy height applications. Remote Sensing Applications: Society and Environment, **35**: 101266. doi:10.1016/j.rsase.2024.101266.

Virkkala, A.-M., Aalto, J., Rogers, B.M., Tagesson, T., Treat, C.C., Natali, S.M., et al. 2021. Statistical upscaling of ecosystem CO2 fluxes across the terrestrial tundra and boreal domain: regional patterns and uncertainties. Global Change Biology, **27**: 4040–4059. doi:10.1111/gcb.15659.

Wagner, J., Martin, V., Speetjens, N.J., A'Campo, W., Durstewitz, L., Lodi, R., et al. 2023. High resolution mapping shows differences in soil carbon and nitrogen stocks in areas of varying landscape history in Canadian lowland tundra. Geoderma, **438**: 116652. doi:10.1016/j.geoderma.2023.116652.

Walker, X.J., Alexander, H.D., Berner, L.T., Boyd, M.A., Loranty, M.M., Natali, S.M., and Mack, M.C. 2021. Positive response of tree productivity to warming is reversed by increased tree density at the Arctic tundra–taiga ecotone. Canadian Journal of Forest Research, **51**: 1323–1338. doi:10.1139/cjfr-2020-0466.

Walker, X.J., Baltzer, J.L., Bourgeau-Chavez, L., Day, N.J., Dieleman, C.M., Johnstone, J.F., et al. 2020. Patterns of ecosystem structure and wildfire carbon combustion across six ecoregions of the North American Boreal Forest. Frontiers in Forests and Global Change, **3**. doi:10.3389/ffgc.2020.00087.

Westoby, M.J., Brasington, J., Glasser, N.F., Hambrey, M.J., and Reynolds, J.M. 2012. 'Structure-from-motion' photogrammetry: a low-cost, effective tool for geoscience applications. Geomorphology, **179**: 300–314. doi:10.1016/j.geomorph.2012.08.021.

White, J.C., Wulder, M.A., Hobart, G.W., Luther, J.E., Hermosilla, T., Griffiths, P., et al. 2014. Pixel-based image compositing for large-area dense time series applications and science. Canadian Journal of Remote Sensing, **40**: 192–212. doi:10.1080/07038992.2014.945827.

Wilmking, M., Harden, J., and Tape, K. 2006. Effect of tree line advance on carbon storage in NW Alaska. Journal of Geophysical Research: Biogeosciences, **111**. doi:10.1029/2005JG000074.

Wojcik, R., Palmtag, J., Hugelius, G., Weiss, N., and Kuhry, P. 2019. Land cover and landform-based upscaling of soil organic carbon stocks on the Brøgger Peninsula, Svalbard. Arctic, Antarctic, and Alpine Research, **51**: 40–57. doi:10.1080/15230430.2019.1570784.

Ziegler, S.E., Benner, R., Billings, S.A., Edwards, K.A., Philben, M., Zhu, X., and Laganière, J. 2017. Climate warming can accelerate carbon fluxes without changing soil carbon stocks. Frontiers in Earth Science, **5**. doi:10.3389/feart.2017.00002.

Zona, D., Lipson, D.A., Zulueta, R.C., Oberbauer, S.F., and Oechel, W.C. 2011. Microtopographic controls on ecosystem functioning in the Arctic Coastal Plain. Journal of Geophysical Research, **116**. doi:10.1029/2009JG001241.